Historical Perspective

Coalescence of surface bubbles: The crucial role of motion-induced dynamic adsorption layer

Jan Zawala [a,b,*], Jonas Miguet [d], Preetika Rastogi [b,c], Omer Atasi [d], Mariusz Borkowski [a], Benoit Scheid [d], Gerald G. Fuller [b]

[a] Jerzy Haber Institute of Catalysis and Surface Chemistry Polish Academy of Sciences, ul. Niezapominajek 8, 30-239 Krakow, Poland
[b] Department of Chemical Engineering, Stanford University, Stanford, CA 94305, USA
[c] Department of Chemical Engineering, Indian Institute of Technology, Chennai 600036, Tamil Nadu, India
[d] TIPs, Fluid Physics Unit, Université Libre de Bruxelles, B-1050 Bruxelles, Belgium

ARTICLE INFO

Keywords:
Bubble
Coalescence
Dynamic adsorption layer
Foam film
Interferometry
Drainage
Direct numerical simulations

ABSTRACT

The formation of motion-induced dynamic adsorption layers of surfactants at the surface of rising bubbles is a widely accepted phenomenon. Although their existence and formation kinetics have been theoretically postulated and confirmed in many experimental reports, the investigations primarily remain qualitative in nature. In this paper we present results that, to the best of our knowledge, provide a first quantitative proof of the influence of the dynamic adsorption layer on drainage dynamics of a single foam film formed under dynamic conditions. This is achieved by measuring the drainage dynamics of single foam films, formed by air bubbles of millimetric size colliding against the interface between n-octanol solutions and air. This was repeated for a total of five different surfactant concentrations and two different liquid column heights. All three steps preceding foam film rupture, namely the rising, bouncing and drainage steps, were sequentially examined. In particular, the morphology of the single film formed during the drainage step was analyzed considering the rising and bouncing history of the bubble. It was found that, depending on the motion-induced state of adsorption layer at the bubble surface during the rising and the bouncing steps, single foam film drainage dynamics can be spectacularly different. Using Direct Numerical Simulations (DNS), it was revealed that surfactant redistribution can occur at the bubble surface as a result of the bouncing dynamics (approach-bounce cycles), strongly affecting the interfacial mobility, and leading to slower rates of foam film drainage. Since the bouncing amplitude directly depends on the rising velocity, which correlates in turn with the adsorption layer of surfactants at the bubble surface during the rising step, it is demonstrated that the lifetime of surface bubbles should intimately be related to the history of their formation.

1. Introduction

The motion of an air bubble in a Newtonian liquid can be divided into two limiting cases. The first case concerns so-called "clean" bubble rising due to gravity in clean liquids, free of surface-active molecules. The second case is encountered in solutions of surface-active species. In the former, the interface of the bubble and the continuous phase (air/liquid interface) is fully mobile leading to a lower viscous drag at the bubble surface as compared to that when surface-active species are present at the bubble interface. The rising velocity in the former case is higher in comparison to a solid sphere of identical size and density [1–5]. Similar to the latter case, it was theoretically shown by Frumkin

and Levich [5,6] that the convective-diffusive kinetics, involving adsorption and desorption of surfactant molecules at the bubble surface, leads to a surface concentration gradient on a moving bubble, reducing its surface mobility. This situation is schematically illustrated in Fig. 1A. As a consequence of the bubble motion, the surface concentration of surfactants at the bubble rear pole is higher than the equilibrium value, while the top pole is largely depleted. In other words, the adsorption coverage at the bubble surface increases in the direction opposite to the bubble motion. In a limiting case, the leading part of the bubble can be almost free of surfactant molecules and hence fully mobile, whereas the rear part (so-called rear stagnant cap, RSC) is covered by a compressed adsorption layer and hence immobile [1,2,7–12]. This uneven
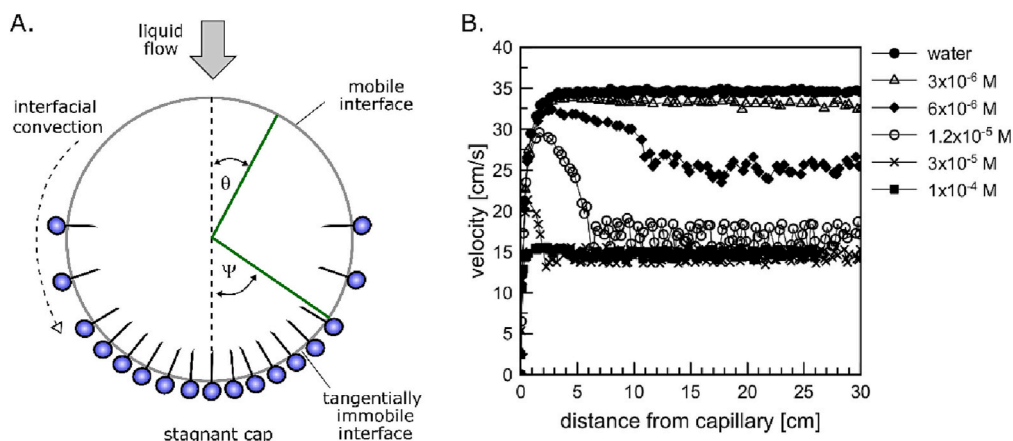

Fig. 1. (A) Dynamic adsorption layer according to the Rear Stagnant Cap (RSC) theory, where Ψ is the polar angle of the RSC, indicating the immobile part of the liquid/gas interface ([9]), (B) local velocity profiles (LVP) for an air bubble of radius 0.74 mm rising in n-octanol solutions of different concentrations (based on data taken from [3]).

distribution of surfactant molecules at the bubble surface leads to Marangoni stresses causing a retardation of the liquid/gas interface mobility, an increased drag coefficient and, consequently, a lower bubble rising velocity. The uneven adsorption layer formed under the above-described dynamic conditions is called the dynamic adsorption layer (DAL) [2,9].

The existence and kinetics of the development of the DAL, as well as the implication of its presence on the stability of liquid foam films once the bubble has collided with the solution/air interface, has been a subject of many theoretical and experimental studies [2,7–10,12–21]. It must however be underlined that all the experimental attempts undertaken so far were qualitative, and no direct evidence has been reported to date. The presence of theoretically postulated motion-induced DAL on the surface of a rising bubble has been confirmed in experiments, where the variations of the rising velocity of a bubble with time or distance traversed in a liquid column were determined [2,9,14,16,22–24]. It is known that the measurements of the bubble local velocity profiles (LVP) offer an insight into the development of the DAL structure and kinetics, which no other technique provides. An example of the LVP determined for n-octanol solutions of different concentrations and bubble of radius 0.74 mm is given in Fig. 1B [3]. It was experimentally observed that after the acceleration stage and before reaching the steady-state conditions (i.e., terminal velocity), the bubble velocity can pass through a maximum, the height and width of which are proportional to the solution concentration [3,4,9,18,25–29]. Next, when steady-state conditions are reached, the bubble rises with a terminal (constant) velocity, which is an indication of the existence of the fully developed DAL structure at its surface. Therefore, it is commonly accepted that the LVP, reflecting the parameters of a single bubble motion, is an indirect measure of the kinetics of the DAL formation [3,6,8,16] and dynamic changes in the drag coefficient. As seen in Fig. 1B for all studied n-octanol concentrations (in the range 3×10^{-6} - 1×10^{-4} M) and the particular bubble radius (0.74 mm), a distance of 15 cm was sufficient for steady DAL establishment [3,4]. The value of this distance, however, increases with the bubble radius [16,30].

The presence of DAL was also confirmed in experiments, where the stability of single foam bubbles [31–34] and wetting [7,14,35,36] films formed by a colliding bubble were assessed. In these experiments, the distance L between the bubble formation point (orifice) and the liquid/air or liquid/solid interfaces was adjusted to reflect the different stages of the DAL development at the rising bubble surface before its collision and liquid film formation. Two lengths of liquid columns were used for this purpose (short, where L was of the order of few centimeters, and long, with L ranging between 15 and 40 cm). It was found that the time of rupture of a single liquid film formed by the colliding bubble was

significantly shorter for high values of L, despite the fact that a considerable increase in the equilibrium adsorption coverage at the bubble surface was expected since the bubble travelled a longer distance in the liquid column of a higher length L. The results suggested that despite the higher coverage, the drainage rate of the liquid film was higher in the longer column. This argument was used as a proof of a higher degree of mobility and the existence of a zone of depleted surfactant concentration at the bubble apex. This experimental argument, however, was based on the measurement of an indirect quantity, namely the lifetime of the bubble at the solution surface. It was supplemented by theoretical calculations using a model assuming wave-induced foam film drainage by Sharma and Ruckenstein [37], with the assumption of a non-uniform adsorption coverage at a liquid/gas interface as described by Ivanov et al. [38]. No experimental evidence of this phenomenon during the time evolution of the liquid film drainage was available to show variations of the bubble interface mobility. Recently, a new interesting experimental method, called "bubble in flow field" was reported [8], which mimics the situation of a rising bubble in surfactant solutions. A bubble was fixed at the capillary tip and the influence of the liquid flow, over the bubble surface, on the dynamic surface tension was determined using a capillary pressure tensiometer. Unfortunately, the experiments did not provide straightforward evidence for the DAL formation because, as the authors concluded, "…the redistribution of pre-adsorbed surfactants does not seem significant or does not lead to a measurable pressure change …". Therefore, the more direct quantitative proof of this phenomenon has not yet been obtained.

In all the experiments aimed at obtaining a direct proof of the DAL presence at a rising bubble surface by assessment of a single foam stability reported in the literature so far, the step of bubble bouncing, occurring after the collision with a solution surface, has been disregarded. It was assumed instead that due to large differences between timescales of bubble bouncing (up to 100–150 ms [39,40]) and foam film drainage formed by the colliding bubble (usually seconds and even minutes for surfactant solutions [41–43]), the bouncing should not significantly affect the DAL structure and, hence, the interfacial mobility. Although not obvious (due to negligible bubble mass), bubble bouncing is a well-established effect, discovered thanks to the use of high-speed videography [44]. The bubble bouncing kinetics at various interfaces has been widely investigated experimentally and theoretically [45–53], to elucidate the bubble coalescence dynamics and hence the mechanism of liquid film rupture. It is commonly accepted that bubble bouncing is a consequence of exchange between the kinetic energy associated with its motion (and accumulated in the liquid phase) and surface energy, which increases at the moment of collision, due to the bubble area enlargement [48,54,55]. Consecutive approach-bounce
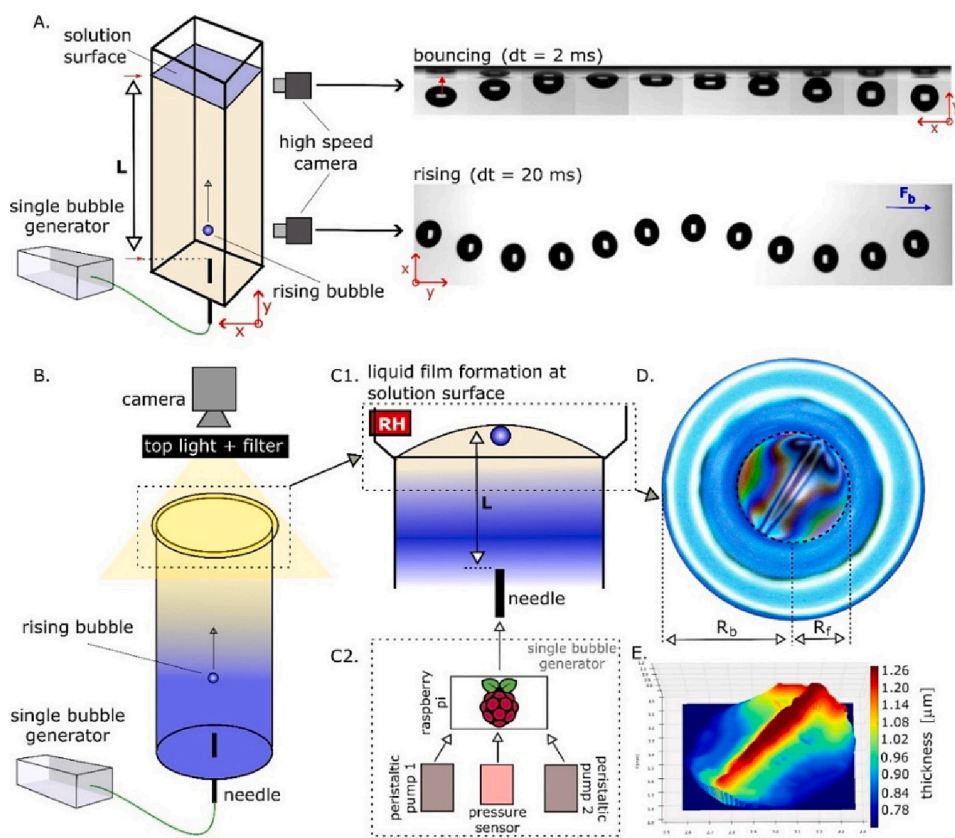
Fig. 2. Schematic illustration of the experimental set-up comprising glass liquid column either with square (A) or circle (B) cross-section, with the needle sealed at the bottom. A single bubble of radius R_b was generated using an automatic single bubble generator (C2). The rising step of the bubble was monitored as a function of distance from the capillary tip using high speed camera (A). Collision of a bubble with the solution surface located at two different distances ($L = 1$ and 40 cm) from the needle tip (A and B) was monitored either by (A) high speed camera to obtain data on the bubble bouncing dynamics and (B) DFI device (top CCD camera with filter) allowing for determination of interference patterns inside the foam film of radius R_f, and its thinning dynamics (D). Post-processed spatial distribution of thickness of the foam film (E). The relative humidity was measured by the RH sensor mounted above the solution surface (C1).

cycles of the bubble, related to this phenomenon, are associated with viscous losses causing a decrease in the bouncing amplitude and eventual capture of the bubble beneath the interface, where a liquid film is formed, and drainage initiates. For pure liquids, this picture was experimentally demonstrated both at liquid/gas and liquid/solid interfaces, where it was shown that supply of the kinetic energy to the system from an external source can cause formation of so-called immortal bubbles, bouncing indefinitely even at the surface of silicone oils of very low surface energy, of pure water or even of highly hydrophobic substrate [40,56–58]. In surfactant solutions, all the experimental and theoretical attempts were related to the investigation of bubble bouncing dynamics by assessment of the so-called restitution coefficient, which compares the rebound and approach velocities [50,59–63]. It was shown that the ability of the bubble to bounce from an interface is related to the degree of fluidity of the two interacting interfaces [64]. Moreover, as reported, due to lower bubble surface mobility, the bubble bouncing amplitude and duration decrease with increasing surfactant concentration and can be practically totally damped above a threshold concentration value, as a results of lower bubble approach speed and surface deformability, related to its immobilization as well as higher viscous dissipation of energy[23,61,65–69]. Increase in the concentration of surfactant in solution causes a decrease in restitution coefficients [70]. Due to lack of sufficient experimental tools for direct estimation of variations in surfactant distribution over the bouncing bubble surface, this important problem remains very poorly examined.

In this work, we present the experimental results on the influence of the distance traversed by a single bubble in a column filled with a surfactant solution (n-octanol - fatty alcohol chosen as a simple model of surface-active agent) on the time-evolution of the thickness of a single foam film formed at a free solution surface. Every step of the bubble's journey, from its creation and detachment to its coalescence at the surface, through the rising, bouncing and thinning steps are

characterized experimentally and thoroughly examined. The aim of this paper is to study the influence of the non-homogeneous coverage of surfactants along the rising bubble surface (the DAL) on the drainage of the subsequently formed foam film at the solution surface. In our studies we adapted the experimental approach reported by Jachimska et al. [31,33] and Warszyński et al. [32], and supplement it with independent interferometry measurements, allowing direct determination of a single foam film drainage dynamics (after its formation by a bubble of relatively large size – radius 1.04 mm - and Reynolds numbers ranging between ca. 350–700), with the additional possibility of visualizing the liquid film morphology. Two different release depths for the bubbles have been prescribed, i.e. 1 cm (short column) and 20 or 40 cm (long column), in order to investigate the effect of a presumably different DAL on the bubble bouncing dynamics and liquid film drainage rates. The experimental investigations have been supplemented by Direct Numerical Simulations (DNS) allowing for reproduction of the bubble rising and bouncing steps, and providing valuable informations on the redistributions of surfactants during these steps. Overall, these results provide strong confirmation of the existence of the DAL on the rising bubble interface, which will be used to provide a plausible explanation of our results.

2. Experimental approach

2.1. Integrated set-up

Similar to many other experimental investigations, motion parameters of a single bubble rising and colliding with air/n-octanol solution interfaces were determined by means of video observations and image analysis [12,16,41,71]. Our experimental set-up is presented schematically in Fig. 2A. More details on the measurement methodology as well as algorithms used for determination of a bubble velocity were published elsewhere [22]. Briefly, a single bubble of equivalent radius R_b

was formed at a steel needle tip (inner diameter $d_c = 0.21$ mm) in a liquid column of square cross-section (40 × 40 mm). To maintain controlled release time delays between two successive bubbles (Δt_b), an automated bubble generator, the details of which can be found in [72], was employed. The growth time for a bubble was 100 ms, small enough to avoid full coverage of the interface by surfactants before release (see below) Motion of a single bubble released from the needle tip was monitored at the distance of 20 cm, using side high-speed camera (SpeedCam MacroVis, 100 frames per second). This distance was far enough for a bubble of sufficient size to reach its terminal velocity (steady-state conditions) in all studied cases (see Fig. 4C). Bubble velocities were calculated from the spatial evolution of its geometrical center position in time (considering only the vertical coordinate - $y_c(t)$) by a frame-by-frame analysis of the recorded images (using script written in Python 3.7). Bubble collision with the solution surface was recorded by this same high-speed camera with recording frequency increased to 1000 fps. The bubble dynamics beneath the air/solution interface were determined for two distances (L) covered by the bubble from the moment of its release to the moment of collision, namely: 1 cm (short column) and 20 cm (long column). The distance L was adjusted by tuning the volume of liquid in the column.

Details on materials used in the experiments are provided in Appendix A.

2.2. Dynamic fluid-film interferometry (DFI)

A schematic illustration of the set-up used to determine the drainage dynamics of a single foam film formed by a bubble colliding upon the liquid bath surface is presented in Fig. 2B. Similar to the experiments described above (bubble motion parameters determination), single bubbles of identical equivalent radii R_b (1.04 ± 0.04 mm) were used. The bubble was formed at the needle tip mounted at the bottom of the round glass columns of two different lengths, where the distance (L) covered by the bubble from the moment of its release to the moment of liquid film formation was equal to 1 cm (short column) and 40 cm (long column). According to the rear-stagnant cap theory, after terminal velocity establishment (under steady state conditions) the architecture of the dynamic adsorption layer does not change with the distance travelled by a bubble in solution of soluble surfactants (due to equilibrium between adsorption/desorption processes), therefore similar DAL states (and resultant surface concentrations) could be assumed both for $L = 20$ and $L = 40$ cm. The thinning dynamics of the foam (thin) film of lateral extension R_f was then measured using the Dynamic Fluid-Film Interferometer (DFI), which construction specific details were described elsewhere [73–75] and in the references therein. After its release from the needle tip and free gravity-driven rise in the liquid column, the bubble enventually partially protrudes through the surface, thus forming a thin liquid film (foam film). During the experiments reported in this paper, the original DFI set-up was modified to be suitable for the observation of the interference patterns observed at the surface of the film when appropriately illuminated with white light. In addition, the relative humidity (RH) above the liquid bath was monitored using a RH digital sensor. More details about the DFI procedure and liquid film thickness measurements are given in Appendix A (section A2 and A3).

2.3. Adsorption kinetics

To estimate concentration-dependent adsorption kinetics of n-octanol molecules at the liquid/gas interface, the freely available software developed by E. Aksenenko [76] was applied. The literature data for the parameters of the Frumkin isotherm, given by the following relations [77,78]:

$$bc = \frac{\Gamma\omega}{1 - \Gamma\omega}e^{(-2a\Gamma\omega)} \tag{4}$$

Table 1
Literature parameters [22] of the Frumkin adsorption isotherm used in adsorption kinetics calculations.

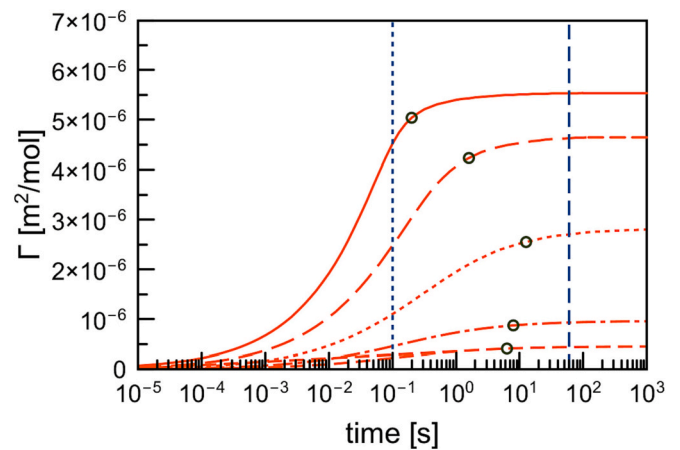| b [dm³/mmol]	1.34
ω [m²/mol]	1.60×10^5
Γ_∞ [mol/cm²]	6.25×10^{-10}
a	1.0
E_s [kJ/mol]	2.5

Fig. 3. Variations of calculated surface concentration as a function of time for all studied n-octanol bulk concentrations (short dash line - 5×10^{-5} mol/dm³, dash-dot line - 1×10^{-4} mol/dm³, dot line - 2.5×10^{-4} mol/dm³, long dash line - 5×10^{-4} mol/dm³, solid line - 1×10^{-3} mol/dm³) – vertical doted and dashed lines indicate, respectively, the bubble growth time and the minimum equilibration time of the bath surface between each experiment. Points mark the time needed to reach 90% of Γ_{eq} value corresponding to the plateau value.

$$\Pi = -\frac{RT}{\omega}\left[ln(1 - \Gamma\omega) + a(\Gamma\omega)^2\right] \tag{5}$$

were used in calculations. These parameters are tabulated in Table 1. In Eqs. (4)–(5), Π is the surface pressure, R is the gas constant, T is the temperature, Γ is the surface concentration, ω is the area per one adsorbed molecule in the close-packed monolayer (equal to $1/\Gamma_\infty$), b is the adsorption constant and a is a parameter related to the interaction (with some characteristic energy H_s) between adsorbed molecules, which is proportional to $-H_s/RT$. Using Frumkin isotherm constants and assuming diffusion-controlled adsorption kinetics, the development of the surface concentration at a liquid/gas interface as a function of time was calculated by numerical solution of the Ward-Tordai eq. [77]:

$$\Gamma(t) = 2\sqrt{\frac{D}{\pi}}\left(c_0\sqrt{t} - \int_0^{\sqrt{t}} c(0, t - t')d\sqrt{t'}\right) \tag{6}$$

where t is time, D is the surfactant diffusion coefficient in the solution, c_0 is the surfactant bulk concentration and $c(0,t)$ is the surfactant concentration in the surface sub-layer. The calculations were performed for flat liquid/gas interfaces (the radius of curvature tending towards infinity). The calculation results for all studied n-octanol concentrations, performed for the parameters obtained from Frumkin isotherm (see Table 1) are shown in Fig. 3. The bubble maximum growth time (100 ms) is marked with dotted vertical line. The vertical dashed line indicates minimum time maintained for bath surface equilibration (minimum time interval between bubble rupture and subsequent bubble arrival). Points indicate the time needed to reach 90% of Γ_{eq} ($\Gamma_{t=\infty}$), which we arbitrarily take as representative of an adsorption timescale.
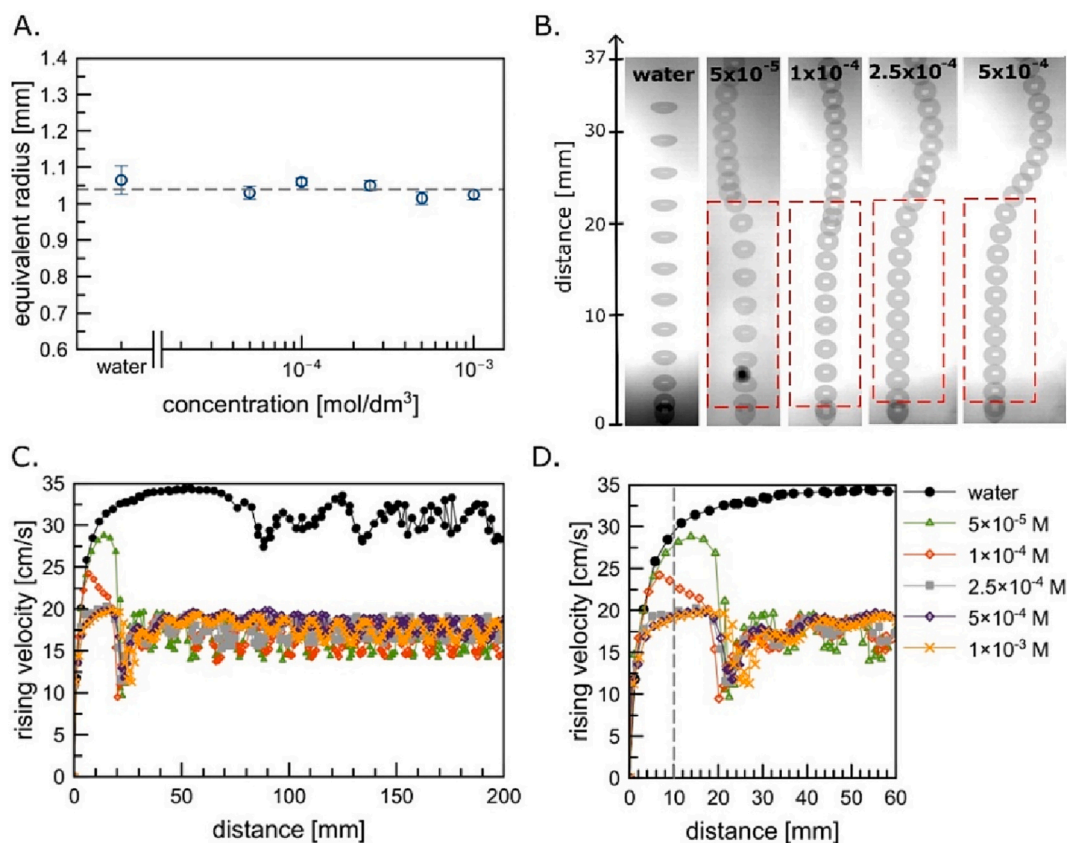
Fig. 4. Data on (A) equivalent radius (R_b) of a rising bubble as a function of n-octanol solution concentration. Bubble snapshots after release from the needle at the origin of the vertical axis) in (B) superimposed by intervals of 10 ms for each full movie frame (37 mm). (C,D) Vertical velocities (y-component) of the rising bubbles as a functions of the distance from the needle tip, showing the acceleration stage (outlined with red dashed line in B), maximum velocity and terminal velocity establishment. (For interpretation of the references to color in this figure legend, the reader is referred to the web version of this article.)

3. Sequential bubble history

3.1. Bubble rising

After release from the needle tip, the bubble accelerates in the liquid. As was previously reported in many papers [2–4,9,79,80], the bubble motion dynamics depend on the concentration of surface-active substances present in an aqueous phase. Fig. 4 presents the data on the motion parameters (local velocity profiles – LVP) of a single bubble observed in our studies. As seen in Fig. 4A, increase in n-octanol concentration did not affect much the R_b values (defined as the radius of the equivalent circle that has a surface area equivalent to the observed bubble), which remained almost constant in all experimental series, essentially because in most of the studies, the generation time (100 ms, see Fig. 3) was faster than the typical adsorption timescale. For the highest concentrations, slight decreases in R_b can be observed due to higher surface concentration, hence lower surface tension. For all cases presented in Fig. 4BCD, a clear bubble acceleration period is observed, magnitude of which determines the value of the bubble maximum velocity. As reported in the literature [3,4,22], the heights and widths of maxima in the LVPs depend on solution concentration. In our case the maxima widths were comparable, while their heights diminished with n-octanol concentration, being the biggest for 5×10^{-5} mol/dm³, intermediate for 1×10^{-4} mol/dm³ and the smallest (or even negligible) and almost constant for 2.5×10^{-4}, 5×10^{-4} and 1×10^{-3} mol/dm³ (compare the areas outlined with red dashed lines in Fig. 4B). It is commonly accepted that the existence of a maximum in the LVP is an indication of formation of the DAL at the bubble surface, where the interface has not been yet immobilized by the surfactant non-uniform distribution and Marangoni effect. Gradual immobilization of the

bubble surface starts just before the maximum, beyond which the bubble enters the deceleration stage, which indicates an increase in the hydrodynamic drag (C_D). Maximum C_D values are reached when the bubble starts to rise with the terminal (constant) velocity. It can be seen in Fig. 4CD that the moment of full immobilization of the bubble surface took place after ca. 30–40 mm for all studied n-octanol concentrations, what means that for distances >40 mm, the bubble velocity was stationary. Observed bubble path instabilities (referred sometimes as Leonardo's paradox [81]) have been the subject of many papers reporting experimental [82–86] as well as numerical studies [85,87–89]. As seen in Fig. 4B, the bubbles adopted a zig-zag path, rather than straight line, even in the case of water (after distance > ca. 50 mm). Detailed analysis of this phenomenon is out of the scope of this paper. It is, however, worth highlighting that, according to the analysis done in the literature on the basis of Galilei ($Ga = \rho\sqrt{gR_b}R_b/\mu$) and Bond ($Bo = \rho gR_b^2/\sigma$) numbers [88,90], describing the ratio of the gravitational force to the viscous and surface tension forces, respectively, our bubbles should rise in asymmetric and oscillatory regimes [90]. The oscillatory motion, therefore, is consistent with the observations already reported in the literature.

The LVPs given in Fig. 4C justify the column heights chosen to exhibit the effect of the DAL on the bubble once it reached the solution/air interface. Whatever the concentration, any height above 5 cm is enough to recover a constant ascension velocity and therefore, presumably, a steady adsorption layer. On the other hand, when the column height is 1 cm the velocity for the lowest concentrations is not yet steady and therefore the amount of adsorbed surfactants and their distribution are different from the steady velocity case and depend on concentration.
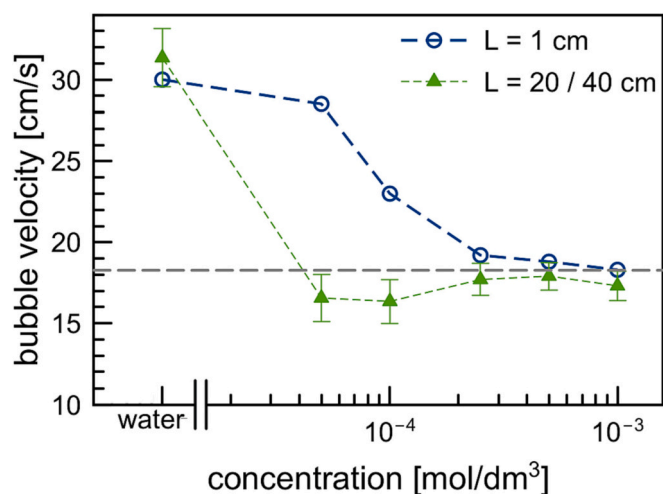
Fig. 5. Bubble velodity at the first collision with the air/liquid interface for the two column heights, as a function of n-octanol concentration.

3.2. Bubble bouncing

Because of the presence of maxima at the LVPs, the bubble velocity at the arrival on the surface differs significantly for the short column as compared to the velocity under steady-state conditions for the long column. Fig. 5 directly presents this comparison. As could be already deduced from the data presented in Fig. 4, the most significant difference in velocities at these distances can be observed for the smallest concentrations (5×10^{-5} and 1×10^{-4} mol/dm^3), where the difference between velocity at the $L = 1$ cm and terminal velocity was equal to ca. 12 and 6.5 cm/s, respectively. For higher concentrations, where the

maxima at the LVPs were hardly definable ($0.25–1 \times 10^{-3}$ mol/dm^3), there was no such a difference.

It was found that these velocity differences have a profound influence on the colliding bubble bouncing dynamics at the air/solution interface. Fig. 6 presents the time evolutions of the bubble geometrical center position (vertical component y_c) and the bubble velocity during collision at the air/solution interface. The moment of bubble collision was adjusted to match the value of time equal to zero, so negative time values correspond to the bubble approach period. Fig. 6AC present the data for $L = 1$ cm, while Fig. 6BD for $L = 20$ cm. Clear differences in bouncing amplitudes and velocities of each subsequent bounce for corresponding concentrations can be observed. Due to significantly higher impact velocities for $L = 1$ cm, the bubble bouncing amplitudes and resultant velocity variations are the most pronounced for concentrations 5×10^{-5} and 1×10^{-4} mol/dm^3. For $L = 20$ cm, no significant differences in bouncing amplitudes and velocity changes can be observed for all ranges of the n-octanol concentrations, due to practically identical impact velocities in all cases (see green triangles in Fig. 5).

3.3. Film drainage

Time evolutions of the average liquid film thickness determined by means of image analysis for concentrations 5×10^{-5}, 1×10^{-4} and 2.5 $\times 10^{-4}$ mol/dm^3 are presented in Fig. 7. Each data point corresponds to the average of the reconstructed thickness maps (an example is given in Fig. 2D and presented in the Appendix A, section A3). For both column lengths, a repetition of the measurements was made with different bubbles and two different experimentalists to show the good reproducibility of the process ($c = 5 \times 10^{-5}$ M). The thinning dynamics for $L = 1$ cm are only weakly affected by the surfactant concentration, as all curves feature a significant overlap. On the other hand, the $L = 40$ cm case shows intrinsically different behaviors when the concentration is
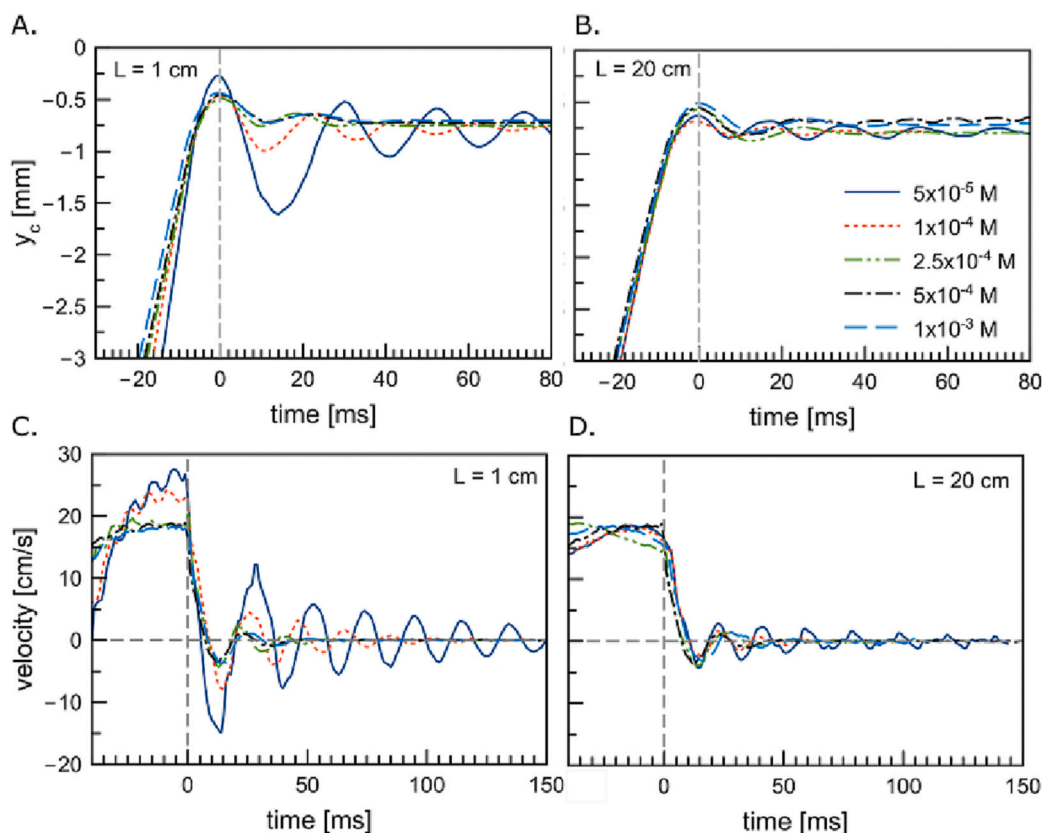

Fig. 6. Variations in the positions of the bubble geometrical center (A, B) and velocity (C, D) as a function of time, during a bubble collision and subsequent bouncing at the air/solution interface for different n-octanol concentrations, for $L = 1$ cm (movies) (A, C) and $L = 20$ cm (B, D) (movies).
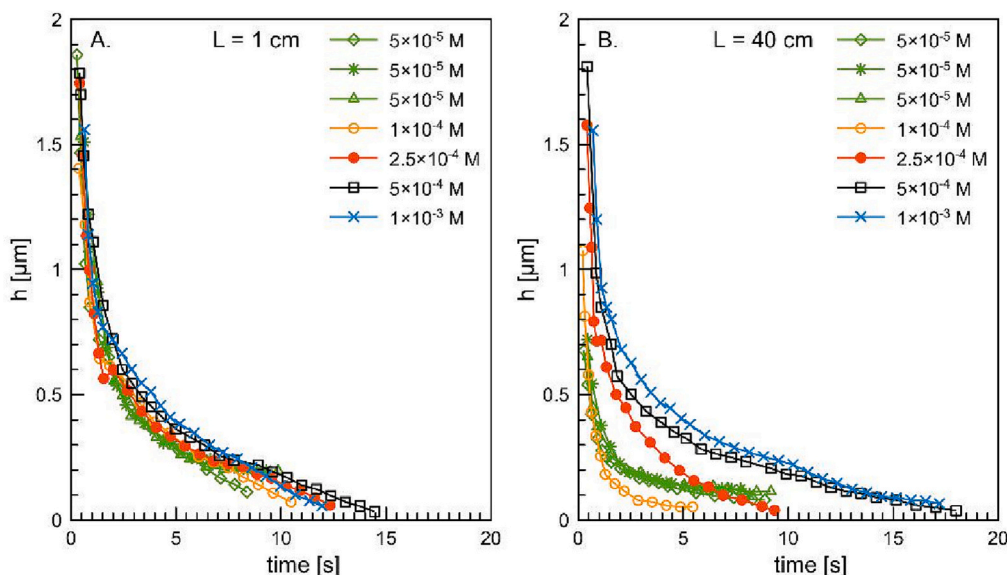
Fig. 7. Time evolution of the foam film thickness for short and long columns.
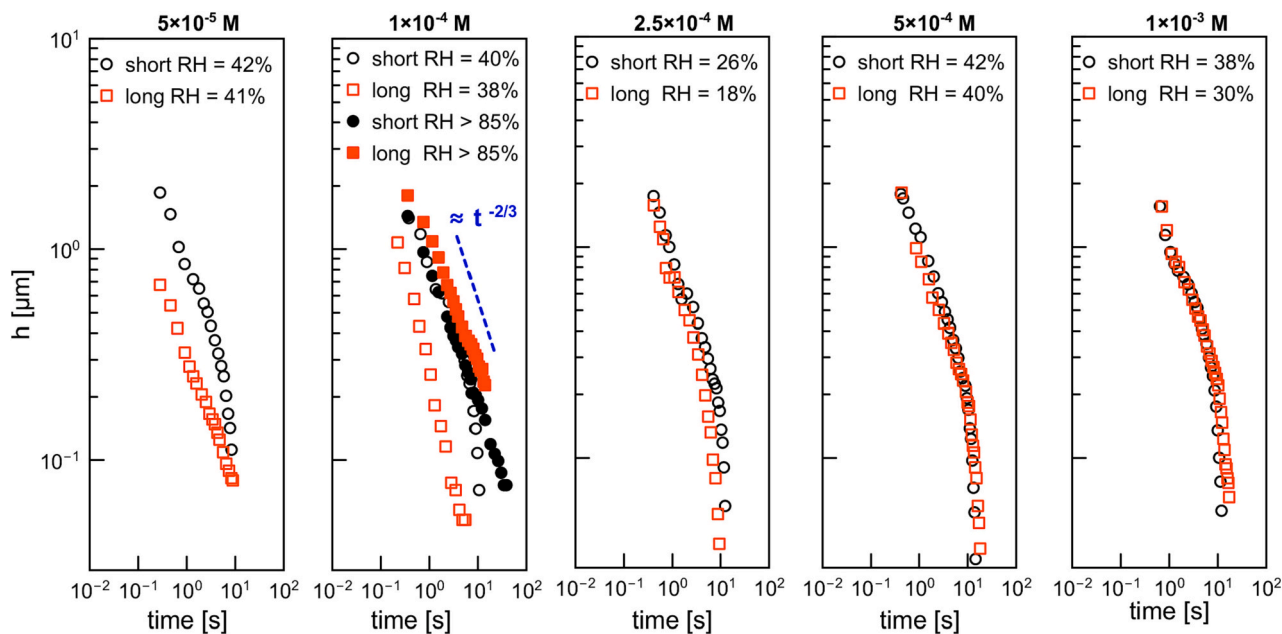

Fig. 8. Log/log representation of thickness measurements as a function of time, for all concentrations and column heights.

changed. In particular, the first measured thickness (the first frame where a clear pattern is observable with DFI) is lower for the two smallest concentrations as compared to the other ones.

Another representation of the thinning data is given in Fig. 8, in logarithmic scales, which compares the thinning behaviors for short and long columns for each concentration. For the three highest concentrations, the thinning dynamics are weakly affected by the column height. This is in line with the fact that the ascension velocity at one centimeter corresponds to the steady rising velocity (Fig. 4) of the system, suggesting that the surfactant concentration distribution is the same for both cases. Correspondingly, the approach velocity is the same for these concentrations (Figs. 4CD and 5) and so are the bouncing dynamics (Fig. 6). On the other hand, for the two smallest concentrations, where significant differences between the approach velocity are recorded at 1 cm and at 40 cm, the thinning dynamics are different in both cases. The first measured thickness is significantly smaller for the long column as

compared to the short one, as if the system was 'shifted' to smaller thicknesses while featuring somewhat similar thinning dynamics revealing a power-law bahaviour, as will be discussed in the next section. The thinning dynamics were also recorded close to saturation conditions for the relative humidity (by closing the measurement cell) to assess the influence of evaporation.

4. Discussion

4.1. Role of the dynamic adsorption layer

Sequences of experimentally acquired photos of a single foam film at its initial stage of drainage for short and long columns for various n-octanol concentrations and a short qualitative analysis are presented in Appendix A (section A3). An important qualitative outcome of these series of images is that for all experiments we observe thin portions of

the film appearing at the bottom of the bubbles and progressively colonizing the entire film. This is reminiscent of the so-called marginal regeneration observed in flat films [91,92] as well as on bubbles [93,94]. These thin film patches arise from the destabilization of the pinch that forms at the connection between the thin spherical cap and the thick meniscus [95]. Its extension is prescribed by the pressure jump between these two zones and determines the magnitude of the pressure gradient that drives the drainage.

Numerous authors have considered the problem of small draining surface bubbles in the presence of surfactants [93,96–98]. By small, we mean that the driving force both for the drainage and the shape of the bubble has a capillary origin. This implies that the bubble has a spherical cap shape beneath the original surface height with an unchanged radius of curvature. The protruding part of the surface bubble, where the thin foam film forms, however, must then have a radius twice as large, since there are two interfaces, to satisfy the equality of the pressure everywhere in the bubble according to: $\frac{4\gamma}{R_{film}} = \frac{2\gamma}{R_b}$. When the film becomes relatively thin, of the order of 1 μm, two contributions must be considered to describe the thinning of the film [99]: the capillary-induced drainage and the evaporation. Lhuissier &Villermaux [93] showed that under experimental conditions similar to our own, the drainage is limited by the existence of a pinch at the transition region between the top of the meniscus that connects the thin film to the bath. This region corresponds to the portion where the capillary pressure gradient between the thin film and the meniscus, that drives the flow, is set. This model provides the best scaling analysis to date to explain the power-law dependence of the thickness to time with an exponent $-2/3$. The data shown in Fig. 8 are all consistent with this dependence of the thickness at early times, as is illustrated with the corresponding slope for $c = 1 \times 10^{-4}$ M. We also observe at later times (this is particularly true at high concentration) a faster thinning regime, which is expected when evaporation starts to overcome the contribution of drainage to the overall thinning of the film. We actually observe this for all experiments far from humidity saturated conditions (the measured relative humidities values RH are given in the legend). The fact that late time thinning is dominated by evaporation is demonstrated for $c = 1 \times 10^{-4}$ M for the short column, when comparing humidity-saturated conditions (RH > 85%) with non-saturation conditions. As seen for RH = 40% the film thickness drops down due to faster evaporation in the late thinning regime, while the film thickness in saturated conditions (> 85%) still follows the power law.

All these considerations suggest a scenario where, rather than impacting the drainage dynamic itself, the DAL presence affects the first instant of the drainage, say the initial thickness of the draining film, that is extremely difficult to access experimentally for the following reasons: (i) when it protrudes through the bath surface, the bubble conserves vibrational motions until the initial kinetic energy is completely dissipated: this renders the focusing of the interferometer complicated, (ii) if, as a crude approximation, we apply a Landau-Levich-Derjaguin model for the initial thickness of the film with an extraction velocity of 0.18 m/s (corresponding to most data, see Fig. 4), we find that the initial thickness is tens micrometers: well beyond the coherence length of visible light and out-of-range for interferometry. This initial thickness is in line with literature data obtained (a few hundreds of milliseconds after protrusion) by measuring the retractation velocity of the hole and applying a Taylor-Culick model to get the thickness [93,99], (iii) the film is still very thick at early times so unlikely to spontaneously burst; manual bursts are doable but not with a good precision and it was only done for $t > 1$ s [99], so the initial draining thickness measurement is not accessible with the Taylor-Culick model.

Describing the whole journey, step by step, first the bubbles are formed and released at the needle tip, which lasts 100 ms. This time scale is short in comparison to the adsorption time scale, so we can consider that small amounts of surfactants are adsorbed at this step. Then, the bubbles rise to the solution surface during a time that scales as $\frac{L}{V_t}$, where $V_t \approx 0.18$ m·s^{-1} is the terminal velocity. The rising time is roughly 60 ms for the short column and >2 s for the long one. During this step, surfactants adsorb onto the surface and are swept towards its bottom as the stagnant cap forms. Next, as the bubble impacts the surface, our measurements show that bouncing occurs only for the short column with the two lowest concentrations: 5×10^{-5} M and 1×10^{-4} M. This is because the velocity of impact, and thus the kinetic energy, is higher in these cases (Fig. 4). These bubbles then experience an inversion of the sense of the flow which should sweep the surfactants towards the bubble apex. We can therefore assume that some surfactants are present in these cases when the thin foam film is formed. On the other hand, when no bouncing occurs, that is, when the impact velocity and the associated kinetic energy are lower (terminal velocity of the rising bubble with fully or at least significantly developed stagnant cap), the upper surface of the bubble, where the foam film is formed, is initially free of surfactant. If the liquid is free of surfactant, no shear occurs on the interfaces and the drainage is expected to be extremely fast. Considering an initial inertia-limited flow, the timescale would be $\sqrt{\frac{\rho R^3}{\gamma}} \sim 10^{-2}$ s. This is contradicted by our experiments since the bubbles live roughly three orders of magnitude longer than this estimate. The DFI images show that there is a pinch at the bottom of the bubbles for all experiments. This pinch was studied theoretically by Aradian et al. [100] in a framework where a no-slip boundary condition was applied (the velocity at the interface is zero). On the other hand, Howell and Stone [101] showed that in the opposite case of a fully mobile film (the shear at the interface is zero), the pinch cannot form because the capillary-driven suction of the fluid is instantaneously transmitted throughout the film. We can argue that (i) if the upper surface of the bubble can be free of surfactant, the free surface, despite its deformation, must be at least partially mobile because marginal regeneration otherwise does not occur, (ii) as the mobile film falls within the meniscus, a local accumulation of surfactants at the bottom of the film leads to a local rigidification of the interface. For these reasons, the necessary quantity of surfactants to obtain a pinch is extremely small but it has a dramatic impact on the system. The model of Lhuissier&Villermaux predicts a lifetime of ~50 s but when accounting for the evaporation, as was done by Poulain et al., we recover timescales in line with the duration of our experiments (~10 s).

The scenario that we propose is therefore that for the three higher concentrations, the adsorption of surfactants is fast enough so that short and long columns present no significant difference. The faster adsorption timescale and rehomogenization of surfactant concentrations on the surface of the newly created thin film led to equivalently fast pinching and therefore equivalent drainage dynamics. On the contrary, for smaller concentrations, significant differences emerge between short and long columns. The long column case features an impact with no bouncing as discussed above. Since the concentrations are small, two arguments plead for a delayed rehomogenization as the new thin film is created: (i) the upper surface of the impacting bubble is full bare at the moment of impact, that is also the moment of the formation of the film (no bounce), (ii) the adsorption rate is lower for lower concentrations, which holds for both interfaces (there is indeed also a depletion of surfactants at the bath surface during the protrusion of the bubble) (iii) the stagnant cap angle on the bubble surface is also smaller for lower concentrations, leading to longer distances to be travelled by the surfactants to reach the thin film region. This delayed rehomogenization supports the scenario that the forming film initially drains without surfactant and therefore without pinch, as for bare bubbles. After few milliseconds, the rehomogenization of the interfaces allows for the formation of the pinch and both marginal regeneration and a dependence $h \propto t^{-2/3}$ are then recovered. Even if this rehomogenization delay only lasts few milliseconds, the drainage being exponential for bare bubbles, it can explain why the first measured thickness with the DFI is approximately twice smaller as compared to essentially all other experiments (see Fig. 8). For the corresponding short-column case, the impact
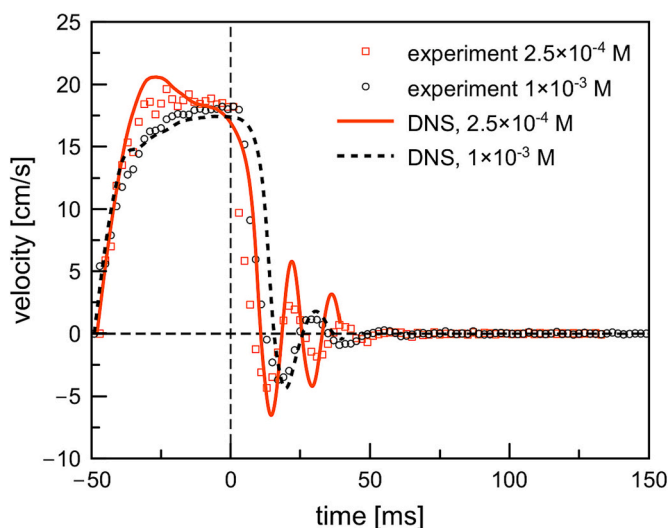
Fig. 9. Result of Direct Numerical Simulations (DNS) of the short-column case for n-octanol concentrations 2.5×10^{-4} M and 1×10^{-3} M (lines – numerical simulations, points – experimental data).

velocity is significantly higher. Because of the higher kinetic energy of these bubbles, pronounced bounces are observed, which leads to a rehomogenization of the surfactant before the thin film is created. The pinching therefore occurs equivalently faster in these situations as compared to experiments at higher concentration.

4.2. Flow redistribution of surfactants at a bubble surface

To visualize the redistribution of surfactant molecules at a bouncing bubble surface a few numerical simulations were conducted using the same numerical approach than the one presented in [102–104], and summarized in Appendix B. Due to computing limitations, the upper surface was treated as a rigid wall (as if the bath surface were non-deformable and rigidified by the presence of surfactants). The simulation results for the short-column case at 1×10^{-3} M and 2.5×10^{-4} M are given in Fig. 9 and compare satisfactorily to the experimental results for the velocity of the bubbles as they approach the interface. For 1×10^{-3} M, the bounces are very well captured by these simulations, both in terms of the amplitudes (and their damping) and frequency. For 2.5×10^{-4} M, the amplitude of the bounces is overestimated, probably because the energy dissipation due to the upper surface deformation is not accounted for (which is more pronounced experimentally in this case because the surface tension is higher for lower concentration). Yet, we consider these simulations as qualitatively representative of the system and we next analyze them in terms of convective transport and
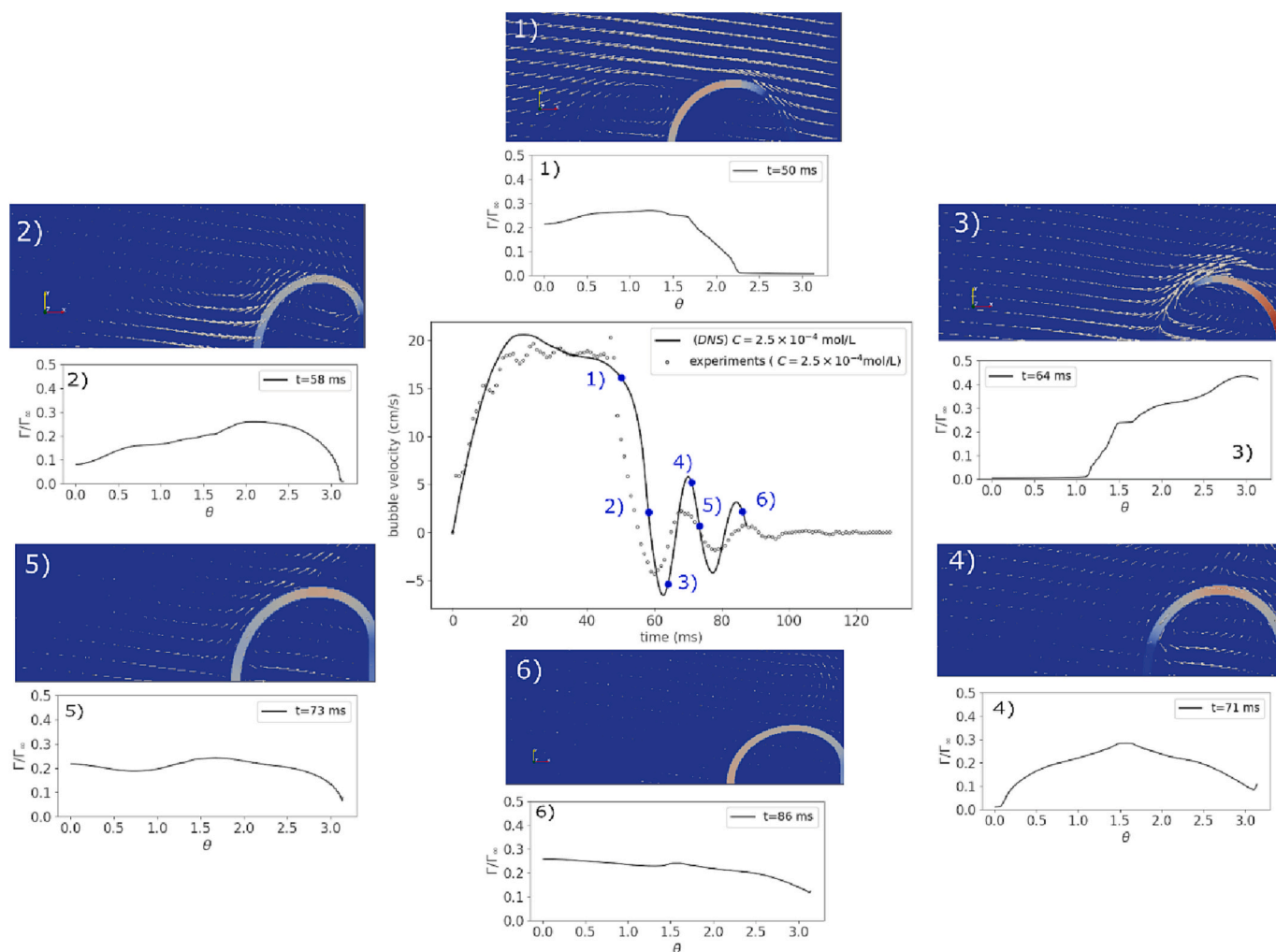

Fig. 10. Close-up on the surfactant distribution along the bubble surface for the n-octanol concentration 2.5×10^{-4} M from the simulations obtained on the basis of Direct Numerical Simulations (DNS). The arrows show the velocity field.

surface distribution of surfactants during this process.

Fig. 10 provides the surfactant distribution along the bubble surface for different times. The first one (1) is the moment just before the deceleration due to the presence of the interface. A very clear stagnant-cap-like structure is observed, with a bare interface near the apex and a covered interface everywhere else, i.e. in the cap region. The smaller surface concentration at the rear compared to, say, $\theta = 1.5 \, rad$, is due to the wake structure that creates a stagnation point where surfactants are swept from the back of the bubble (visible in Fig. 10, panel 1). The second time (2) is when the deceleration of the bubble is such that it is already deformed by the upper surface, but the apex is still free of surfactant. The velocity field shows that the upstream flow due to wake inertia is pushing upwards until time (3), where this flow has pushed almost all surfactants to the apex of the bubble. However, at time (3), the bubble is essentially undeformed because of its backwards motion due to the bounce: the final thin film has not emerged yet. On the contrary, (4), (5) and (6) show that, when the thin film is formed after the bubble has bounced, the rehomogeneization of the surfactants caused by the first bounce lead to an instantaneously populated interface, what is in good agreement with the scenario proposed earlier.

5. Conclusions

Systematic quantitative analysis of three steps related to formation and rupture of a single foam film at a solution surface, namely (i) free rise of an air bubble after release from the orifice, (ii) its collision with a liquid/gas interface and bouncing prior to kinetic energy dissipation, and (iii) drainage of a formed liquid film, allows revealing significant influence of the motion-induced adsorption layer at the bubble surface on the foam film drainage. It was undoubtedly proved based on direct interferometric experiments, that, despite longer residence time of the bubble prior to foam film formation in the longer liquid column (ca. 2 s), a film drainage could be faster comparing to the short column (where the bubble residence time prior to formation of the liquid film was equal to 60 ms, only). This indicates differences in the liquid/gas interface mobility causing different film drainage dynamics, related to more uniform adsorption coverage of the bubble colliding with bath surface located close to the needle tip. Comparison of the experimental observations with result of complementary numerical simulations, allowed for reproduction of all the stages of the bubble's journey and revealed that more uniform surface concentration at the top bubble surface in short column during the drainage stage is caused by the rehomogenization of the surfactant molecules before the thin film is formed. This effect is a consequence of bubble bouncing related to higher bubble impact velocity, causing inversion of the liquid flow, which sweeps the molecules towards bubble upper part during every bubble approach/bounce cycle. Using the single foam film as a sensitive tool for probing the liquid/gas interfaces properties, we unveil a new strong confirmation of existence of the DAL at the rising bubble interface, and both qualify and quantify its effect on the fate of surface bubbles.

Supplementary data to this article can be found online at https://doi.org/10.1016/j.cis.2023.102916.

Data availability

Data will be made available on request.

Appendix A. Coalescence of surface bubbles: the crucial role of motion-induced dynamic adsorption layer

A.1. Materials

N-octanol (simple fatty alcohol having 8 carbon atoms in a hydrophobic chain), purchased from Sigma Aldrich, was used in all experiments as a surface-active agent (purity ≥99%). Hellmanex III® and Mucasol®, commercially available glass cleaning liquids, were purchased from Sigma Aldrich. Milli-Q water (with a resistivity of 18.2 MΩ·cm) was used for the preparation of n-octanol solutions of various concentrations, ranging from 5 $\times 10^{-5}$ to 1×10^{-3} mol/dm^3 as well as for the final cleaning of all the glass components of the experimental set-up in all conducted experiments.

A.2. Dynamic Fluid-Film Interferometry experiments

The experiments were carried out at room temperature (21 °C ± 1°). To acquire the data on ambient relative humidity (RH), an RH sensor (coupled with the Raspberry Pi) was mounted just above the solution surface, acquiring the RH value every 2 s. The experiments were performed either for the liquid column open to the atmosphere, where the ambient relative humidity was ranging between 20 and 40%, or for the column covered by a glass slide. For covered columns, the experiments were started when the RH > 80%.

To faithfully acquire the interference patterns (by the top IDS camera equipped with the LED illumination and Edmund Optics 457/530/628 nm optical filter), the shape of the upper solution/air interface was kept curved in form of a spherical cap, so that the arriving bubble was self-centered at the apex. To extract the time evolution of the thickness of the foam films, an analysis of the reflection interference data, described in detail in ref. [74] (main text), was performed. A typical DFI image is given in Fig. 2D (main text of the paper). One can see the colored interference fringes that are then analyzed to provide a thickness map of the thin film (Fig. 2E in main text of the paper). This is obtained by observing the bubble vertically from the top. The much larger bubble extension, beneath the surface can also be observed, which is reminiscent of the small Bond number of the system (the radius is small as compared to the capillary length but large enough for a thin film to protrude above the bath surface).

The radius of the liquid film (R_f), defined in Fig. 2D (main text of the paper), formed at the solution surface was calculated as:

$$R_f = \left(\frac{F_b R_b}{\pi \sigma} \right)^{1/2} \tag{1}$$

while the bubble radius (R_b) was calculated according to:

$$R_b = \left(\frac{3}{4} \frac{d_c \sigma}{\Delta \rho g} \right)^{1/3} \tag{2}$$

resulting from balancing buoyancy ($F_b = \frac{4}{3} \pi R_b^3 \Delta \rho g$) and capillary forces ($F_c \approx \pi d_c \sigma$), where d_c is the needle tip diameter. The theoretically calculated bubble radius for surface tension $\sigma = 72.4$ mN/m, phases density difference $\Delta \rho = 999$ kg/m^3 and gravity $g = 9.81$ m/s^2 was equal to 1.05 mm. It was found that with MilliQ water, the experimentally determined R_b was equal to 1.04 ± 0.04 mm, i.e. matched perfectly the theoretical value. Moreover, it was found that the average values of the R_f/R_b ratio measured experimentally (image analysis – see Fig. 2D in main text of the paper), were equal to 0.43 ± 0.02 and 0.44 ± 0.04 mm for short and long column respectively, i.e., in perfect agreement with the theoretical predictions calculated according to Eqs. (1)–(2) (using values of surface tension of studied n-octanol solutions). This was a good confirmation that, during the experiments, the whole liquid film area was captured and could be further quantitatively analyzed.

In all experiments, the generation time delay between two successive bubbles (Δt_b), was equal to at least 60 s, and was adjusted according to the bubble lifetime, in order to maintain equilibrium adsorption coverage at the solution surface (i.e. top liquid film interface), which could be disturbed during bubble rupture (coalescence). This time delay was chosen in accordance with the adsorption dynamics of n-octanol described in section 2.3 of the main text. Similarly, the generation time for the bubbles was reduced to 100 ms to be able to consider an initial 'bare' condition for the surfactant coverage (concentration of adsorbed surfactants is zero).

A.3. Analysis of time evolution of thickness of single liquid films formed by a bubble

Sequences of experimentally acquired photos (DFI method) of a single foam film at its initial stage of drainage for short and long columns for n-octanol concentration of 1×10^{-4} mol/dm^3 are presented in Fig. A1A and A1B, respectively. The images for comparable drainage times are shown. The color scale bar on the right of the image sequences illustrates the distribution of the film thickness in microns. The bubble/solution surface collision was adjusted for times equal to $t = 0$ s, which corresponds to the first instance where surface deformation is observed on the DFI images. The first image of each sequence corresponds to the moment of appearance of the interference patterns, which were clear enough for reliable image analysis. As a consequence, the sequence (and quantitative results on film thickness shown later in the paper) are shifted by a fraction of second. This short time shift (< 1 s) is related to the bubble collision, bouncing and motion before reaching the curved solution surface apex. For $L = 1$ cm (Fig. A1A) the interference patterns indicate that the drainage is much more homogenous and symmetrical as compared to that at $L = 40$ cm (Fig. A1B).

The effect of column length in film drainage dynamics for n-octanol concentration of 1×10^{-4} mol/dm^3 is illustrated also in Fig. A2, where chosen sequential images from the entire bubble lifetimes are shown for the short (Fig. A2A) and long (Fig. A2B) columns. In addition, spatial distributions of the film thickness obtained from image analysis are provided (bottom sequence for each column length showing the "maps" of thicknesses and illustrating the film topography at the mentioned time instant). As seen, in all cases the drainage of the film is very dynamic with large thickness inhomogeneities. However, as was already discussed above, the interference patterns for $L = 1$ cm are initially more symmetrical. After ca. 4 s they break into more random and complex shapes.
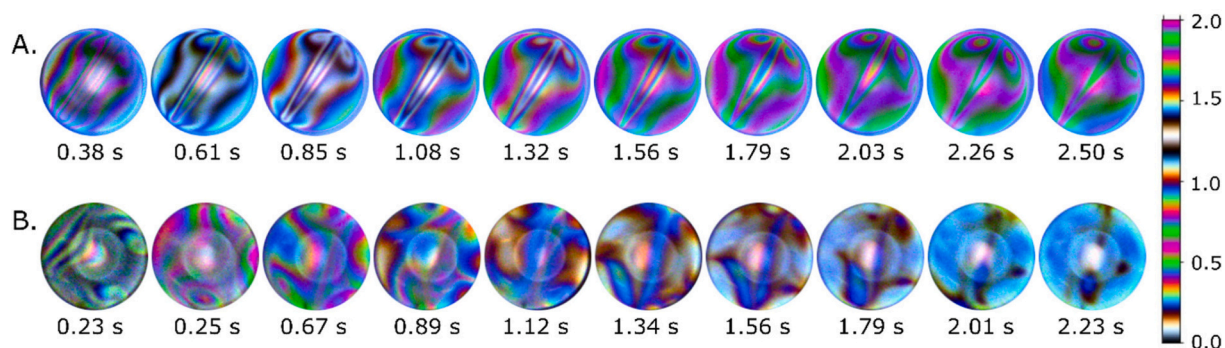

Fig. A1. Sequence of experimentally acquired DFI images of a foam film illustrating initial stage of its drainage in (A) short column and (B) long column at n-octanol solution of concentration 1×10^{-4} mol/dm^3 (see movie in the supplementary material). Values of time from the moment of the bubble collision and liquid film formation are given below each image.
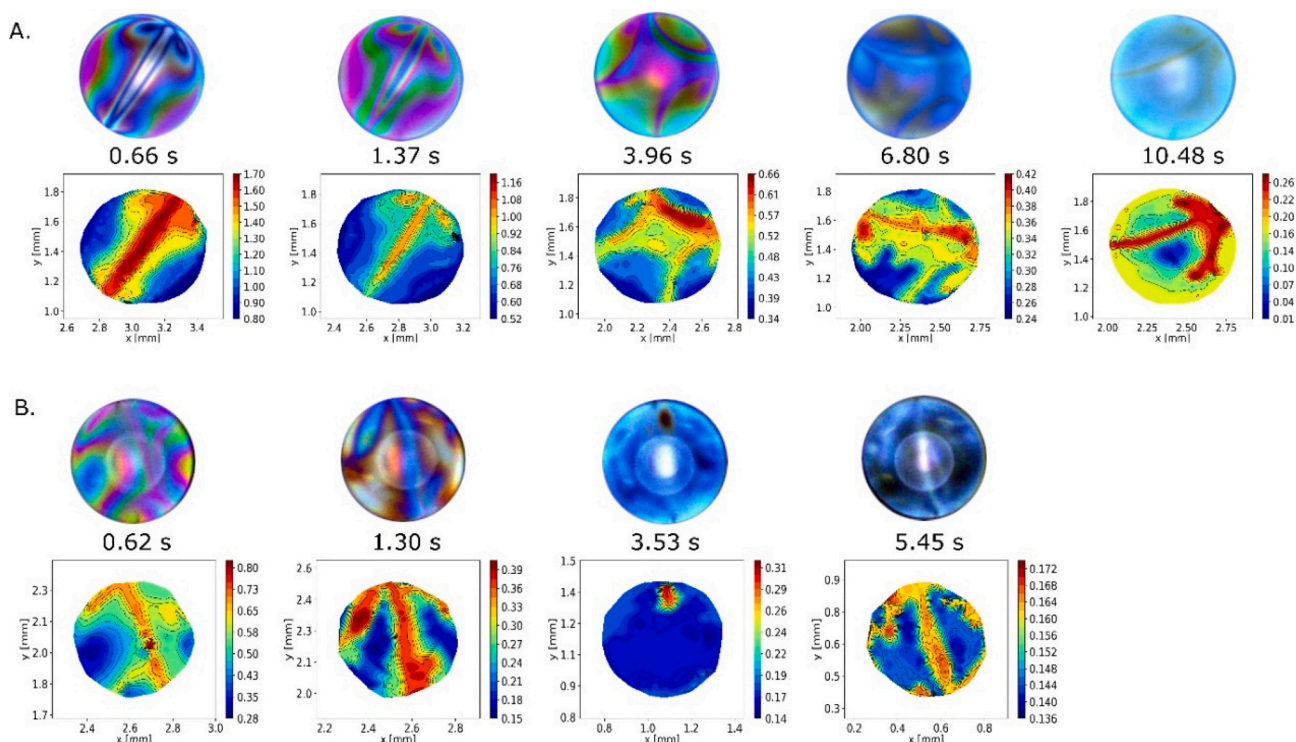
Fig. A2. Sequence of DFI images and corresponding color maps, illustrating spatial distribution of the thickness of a single foam film formed at 1×10^{-4} mol/dm^3 n-octanol solution in (A) short column and (B) long column. Values of time from the moment of the bubble collision and liquid film formation are given below each image.

Similar qualitative analysis for 5×10^{-4} mol/dm^3 n-octanol solution is presented in Fig. A3 for comparison (for $t < 3$ s). In this case, the interference patterns indicate slower drainage for both L values, which seem to be of similar rate. It is to be noted that for $L = 40$ cm, patterns at 5×10^{-4} mol/dm^3 n-octanol concentration are much more symmetrical, compared to the corresponding case in 1×10^{-4} mol/dm^3. Comparison of the last image of each sequence in Fig. A3A and A3B ($t \sim 2.5$ s) with the color scale bar suggests, however, that even at 5×10^{-4} mol/dm^3 n-octanol concentration, drainage rate is a bit higher for $L = 40$ cm. This effect is, however, more subtle compared to the lower concentration (1×10^{-4} mol/dm^3).
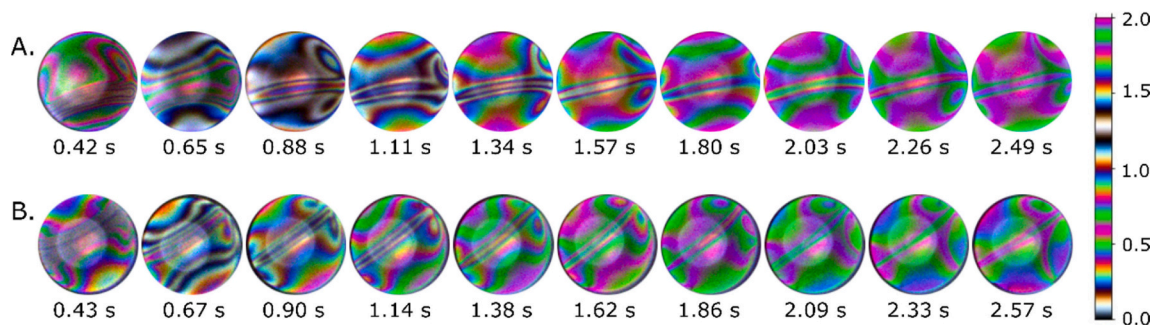

Fig. A3. Sequence of experimentally acquired DFI photos of a foam film illustrating initial stage of its drainage in (A) short column and (B) long column at n-octanol solution of concentration 5×10^{-4} mol/dm^3 (see movie in the supplementary material). Values of time from the moment of the bubble collision and liquid film formation are given below each image.

Appendix B. Coalescence of surface bubbles: the crucial role of motion-induced dynamic adsorption layer

This appendix gives information about the geometry and parameters that were used to obtain the simulation results presented in Figs. 12 and 13 of the main text. It also gives a summary of the numerical method.

B.1. Geometry

The geometry consists of an axi-symmetric bubble at a vertical distance of $L = 5d$ from a solid wall, where $d = 2$ mm is the bubble diameter. At initial time, the liquid contains surfactants at concentration C_0, whereas the bubble surface is clean $\Gamma_0 = 0$ mol/m^3.
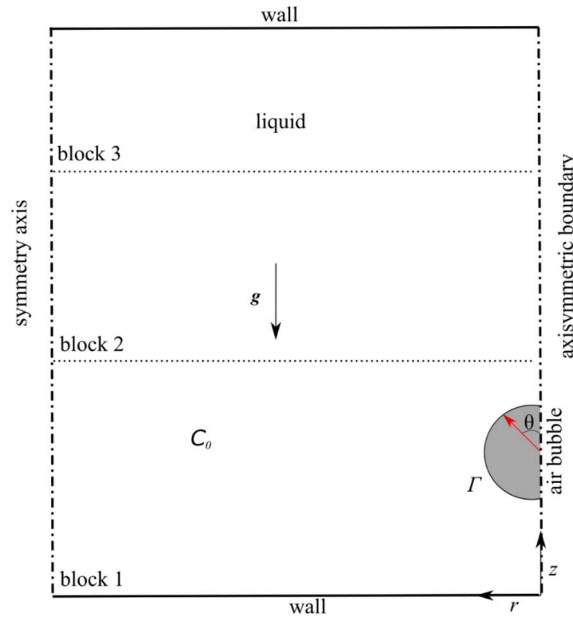
Fig. B1. Schematic of geometry of the computational domain used for the simulation. An initially spherical bubble with a diameter $d = 2$ mm is initialized at a distance of 10 mm from a solid surface. The bubble is immersed in a liquid (aqueous octanol solution) that has an octanol concentration of C_0. Gravity is acting downwards. The computational domain is divided into 3 blocks along the r and z directions. For the sake of clarity, only the blocks along the z direction are depicted. The details of each blocks is given in Table 1.

B.2. Computational mesh

The mesh that was retained for the simulation consists of $n_z = 1170$ and $n_r = 400$ cells along the z and r direction respectively (see Fig. B1). The resolution of the film drainage process requires a fine mesh to resolve the capillary force and viscous stress in the film region. To have a fine mesh in the film region, an arithmetic evolution of the mesh size Δz and Δr was imposed. Practically, the domain was divided into 3 blocks in both the r and z directions (see Fig. B1). In each block an arithmetic sequence is used to generate the mesh, where the mesh is finer near the upper wall and near the bubble (see Table B1). For instance, for the first block in the z direction this gives

$$\Delta z_i = \Delta z_0 + q.i$$

and

$$l_1 = \sum_{i=0}^{i=N} \Delta z_i$$

where Δz_0 is the mesh size in the beginning of block 1 (, 2 or 3), Δz_i is the mesh size of the i'th element in the block and q is the common difference of the arithmetic sequence. Knowing the length of the block, l_1, the minimum value of Δz in the block, Δz_0, and number of computational cells in the block, N_1, the unknown q_1 is deduced and the mesh is built as follows:

$$q_1 = 2\frac{l_1 - N_1 \Delta z_0}{N_1(N_1 + 1)}$$

The parameters of the blocks along the z and r directions are summarized in Table B1.

Table B1
Details about the mesh used for the computations. The domain was cut into 3 blocks along the z and r directions respectively (see Fig. 1). Each block was assigned a given length, number of mesh element and a minimum mesh size. Given these parameters, the mesh was build following an arithmetic sequence.

Block number along z direction	Length (l)	Number of mesh element (N)	Minimum mesh size (Δz_0)	Maximum mesh size (Δz_{max})
1	5 mm	243	13.7 μm	27.4 μm
2	4 mm	403	7.1 μm	13.7 μm
3	3 mm	424	7.1 μm	7.1 μm

Block number along r direction	Length (l)	Number of mesh element (N)	Minimum mesh size (Δr_0)	Maximum mesh size (Δr_{max})
1	3.3 mm	194	17.0 μm	17.0 μm
2	3.3 mm	103	30.0 μm	30.0 μm
3	3.3 mm	102	30.0 μm	30.0 μm

B.3. Parameters

The physicochemical parameters used for the simulations are the ones of an aqueous octanol solution (see Table B2). The parameters of the Langmuir adsorption isotherm for this surfactant are summarized in Table B2.

Table B2
Physicochemical properties used for the simulations. The surfactants properties were taken from [B1] and calculated using algorithm described in the section 2.3 of the main text.

Surface tension [mN/m]	Density [kg/m^3]	Viscosity [Pa·s]	Maximum packing concentration [mol/m^2]	Equilibrium adsorption constant [m^3/mol·s]
70	1000	0.001	6.25×10^{-6}	2.4

B.4. The numerical method

Direct numerical simulations were performed by solving the one-fluid formulation of the Navier-Stokes equations coupled with the Level-Set method. We refer the reader to Atasi et al. [B2] and Abadie et al. [B3] for a detailed description of the method and its validation. In short, the Navier-Stokes equations are solved for two Newtonian and incompressible fluids using the finite volume method (second order accuracy in time and space). Continuity is ensured by a projection method, and the capillary contribution is taken into account by the classical continuum surface force method. The position of the interface is followed using the Level-Set method where the transport of the signed distance at the interface is controlled by the redistancing technique. The transport of surfactants in the liquid bulk, at the surface of the bubble and their exchange between the bulk liquid and the surface are solved using an Eulerian formulation of the transport equations [B4]. The Langmuir adsorption isotherm is used to describe the adsorption process and relate surface tension to surface concentration.

B.5. Computational requirements

Simulations were performed on 2 nodes using 72 cores for 3 days.

References

[B1] Chang, Chien-Hsiang, and Elias I. Franses. "Adsorption Dynamics of Surfactants at the Air/Water Interface: A Critical Review of Mathematical Models, Data, and Mechanisms." *Colloids and Surfaces A: Physicochemical and Engineering Aspects* 100 (July 1995): 1–45. doi:https://doi.org/10.1016/0927-7757(94)03061-4.

[B2] Atasi, O., B. Haut, A. Pedrono, B. Scheid, and D. Legendre. "Influence of Soluble Surfactants and Deformation on the Dynamics of Centered Bubbles in Cylindrical Microchannels." *Langmuir* 34, no. 34 (August 28, 2018): 10048–62.

[B3] Abadie, T., J. Aubin, and D. Legendre. "On the Combined Effects of Surface Tension Force Calculation and Interface Advection on Spurious Currents within Volume of Fluid and Level Set Frameworks." *Journal of Computational Physics* 297 (September 2015): 611–36.

[B4] Xu, Jian-Jun, and Hong-Kai Zhao. "An Eulerian Formulation for Solving Partial Differential Equations Along a Moving Interface," Journal of Scientific Computing (December 2003), Vol. 19.

References

[1] Reinhard Miller, Liggieri L. Bubble and drop interfaces. Brill; 2011.

[2] Dukhin SS, Miller R, Loglio G. Physico-chemical hydrodynamics of rising bubble. Stud. Interf. Sci. 1998;6:367–432. https://doi.org/10.1016/S1383-7303(98)80025-2.

[3] Krzan M, Zawala J, Malysa K. Development of steady state adsorption distribution over interface of a bubble rising in solutions of n-alkanols (C5, C8) and n-alkyltrimethylammonium bromides (C8, C12, C16). Colloids Surf. A Physicochem. Eng. Asp. 2007;298:42–51. https://doi.org/10.1016/j.colsurfa.2006.12.056.

[4] Krzan M, Malysa K. Profiles of local velocities of bubbles in n-butanol, n-hexanol and n-nonanol solutions. Colloids Surf. A Physicochem. Eng. Asp. 2002;207:279–91. https://doi.org/10.1016/S0927-7757(02)00163-2.

[5] Levich VG. Physiochemical hydrodynamcis. Prentice-Hall; 1962.

[6] Frumkin AN, Levich VG. The effect of surface active substances on the motion at liquid interfaces. Zh Fiz Khim 1947;21:1183–204.

[7] Niecikowska A, Zawala J, Miller R, Malysa K. Dynamic adsorption layer formation and time of bubble attachment to a mica surface in solutions of cationic surfactants (C<inf>n</inf>TABr). Colloids Surf. A Physicochem. Eng. Asp. 2010;365: 14–20. https://doi.org/10.1016/j.colsurfa.2010.01.038.

[8] Lotfi M, Bastani D, Ulaganathan V, Miller R, Javadi A. Bubble in flow field: A new experimental protocol for investigating dynamic adsorption layers by using capillary pressure tensiometry. Colloids Surf. A Physicochem. Eng. Asp. 2014; 460:369–76. https://doi.org/10.1016/j.colsurfa.2013.11.011.

[9] Dukhin SS, Kovalchuk VI, Gochev GG, Lotfi M, Krzan M, Malysa K, et al. Dynamics of Rear Stagnant Cap formation at the surface of spherical bubbles rising in surfactant solutions at large Reynolds numbers under conditions of small Marangoni number and slow sorption kinetics. Adv. Colloid Interf. Sci. 2015;222: 260–74. https://doi.org/10.1016/J.CIS.2014.10.002.

[10] Ulaganathan V, Krzan M, Lotfi M, Dukhin SS, Kovalchuk VI, Javadi A, et al. Influence of β-lactoglobulin and its surfactant mixtures on velocity of the rising bubbles. Colloids Surf. A Physicochem. Eng. Asp. 2014;460:361–8. https://doi.org/10.1016/J.COLSURFA.2014.04.041.

[11] Zholkovskij EK, Koval'Chuk VI, Dukhin SS, Miller R. Dynamics of rear stagnant cap formation at low Reynolds numbers. 1. Slow sorption kinetics. J. Colloid Interface Sci. 2000;226:51–9. https://doi.org/10.1006/jcis.2000.6786.

[12] Ulaganathan V, Gochev G, Gehin-Delval C, Leser ME, Gunes DZ, Miller R. Effect of pH and electrolyte concentration on rising air bubbles in β-lactoglobulin solutions. Colloids Surf. A Physicochem. Eng. Asp. 2016;505:165–70. https://doi.org/10.1016/J.COLSURFA.2016.03.059.

[13] Manikantan H, Squires TM. Surfactant dynamics: Hidden variables controlling fluid flows. J. Fluid Mech. 2020;892. https://doi.org/10.1017/jfm.2020.170.

[14] Zawala J, Kosior D, Malysa K. Formation and influence of the dynamic adsorption layer on kinetics of the rising bubble collisions with solution/gas and solution/solid interfaces. Adv. Colloid Interf. Sci. 2015:222. https://doi.org/10.1016/j.cis.2014.07.013.

[15] Palaparthi R, Papageorgiou DT, Maldarelli C. Theory and experiments on the stagnant cap regime in the motion of spherical surfactant-laden bubbles. J. Fluid Mech. 2006;559:1–44. https://doi.org/10.1017/S0022112005007019.

[16] Pawliszak P, Ulaganathan V, Bradshaw-Hajek BH, Manica R, Beattie DA, Krasowska M. Mobile or immobile? Rise velocity of air bubbles in high-purity water. J. Phys. Chem. C 2019. https://doi.org/10.1021/acs.jpcc.9b03526.

[17] Zawala J, Todorov R, Olszewska A, Exerowa D, Malysa K. Influence of pH of the BSA solutions on velocity of the rising bubbles and stability of the thin liquid films and foams. Adsorption 2010;16. https://doi.org/10.1007/s10450-010-9232-3.

[18] Malysa K, Krasowska M, Krzan M. Influence of surface active substances on bubble motion and collision with various interfaces. Adv. Colloid Interf. Sci. 2005;114–115:205–25. https://doi.org/10.1016/J.CIS.2004.08.004.

[19] McLaughlin JB. Numerical simulation of bubble motion in water. J. Colloid Interface Sci. 1996;184:614–25. https://doi.org/10.1006/JCIS.1996.0659.

[20] Liao Y, McLaughlin JB. Bubble motion in aqueous surfactant solutions. J. Colloid Interface Sci. 2000;224:297–310. https://doi.org/10.1006/JCIS.2000.6741.

[21] Clift R, Grace JR, Weber ME. Bubbles, drops, and particles (dover civil and mechanical engineering). 1978. p. 380.

[22] Kosior D, Zawala J. Initial degree of detaching bubble adsorption coverage and the kinetics of dynamic adsorption layer formation. Phys. Chem. Chem. Phys. 2018;20:2403–12. https://doi.org/10.1039/c7cp06099h.

[23] Zawala J, Kosior D, Dabros T, Malysa K. Influence of bubble surface fluidity on collision kinetics and attachment to hydrophobic solids. Colloids Surf. A Physicochem. Eng. Asp. 2016;505:47–55. https://doi.org/10.1016/j.colsurfa.2015.12.023.

[24] Luo Y, Wang Z, Zhang B, Guo K, Zheng L, Xiang W, et al. Experimental study of the effect of the surfactant on the single bubble rising in stagnant surfactant solutions and a mathematical model for the bubble motion. Ind. Eng. Chem. Res. 2022;61:9514–27. https://doi.org/10.1021/acs.iecr.2c01620.

[25] Sam A, Gomez CO, Finch JA. Axial velocity profiles of single bubbles in water/frother solutions. Int. J. Miner. Process. 1996;47:177–96. https://doi.org/10.1016/0301-7516(95)00088-7.

[26] Tan YH, Finch JA. Frother structure-property relationship: Effect of hydroxyl position in alcohols on bubble rise velocity. Miner. Eng. 2016;92:1–8. https://doi.org/10.1016/J.MINENG.2016.02.003.

[27] Tan YH, Rafiei AA, Elmahdy A, Finch JA. Bubble size, gas holdup and bubble velocity profile of some alcohols and commercial frothers. Int. J. Miner. Process. 2013;119:1–5. https://doi.org/10.1016/J.MINPRO.2012.12.003.

[28] Krzan M, Malysa K. Influence of frother concentration on bubble dimensions and rising velocities 2002;36(1):65–76.

[29] Krzan M, Lunkenheimer K, Malysa K. On the influence of the surfactant's polar group on the local and terminal velocities of bubbles. Colloids Surf. A Physicochem. Eng. Asp. 2004;250:431–41. https://doi.org/10.1016/J.COLSURFA.2004.05.022.

[30] Zawala J, Swiech K, Malysa K. A simple physicochemical method for detection of organic contaminations in water. Colloids Surf. A Physicochem. Eng. Asp. 2007;302:293–300. https://doi.org/10.1016/j.colsurfa.2007.02.047.

[31] Jachimska B, Warszynski P, Malysa K. Influence of adsorption kinetics and bubble motion on stability of the foam films formed at n-octanol, n-hexanol and n-butanol solution surface. Colloids and Surfaces A. 2001;192(1–3):177–93.

[32] Warszyński P, Jachimska B, Matysa K. Experimental evidence of the existence of non-equilibrium coverages over the surface of the floating bubblevol. 108; 1996.

[33] Jachimska B, Warszyński P, Malysa K. Effects of motion in n-hexanol solution on the lifetime of bubbles at the solution surface. Progr. Colloid Polym. Sci. 2000; 116:120–8.

[34] Borkowski M, Kosior D, Zawala J. Effect of initial adsorption coverage and dynamic adsorption layer formation at bubble surface in stability of single foam films. Colloids Surf. A Physicochem. Eng. Asp. 2020;589:124446. https://doi.org/10.1016/j.colsurfa.2020.124446.

[35] Wiertel-Pochopien A, Zawala J. Rupture of wetting films formed by bubbles at a quartz surface in cationic surfactant solutions. Chem. Eng. Technol. 2019;42: 1371–80. https://doi.org/10.1002/ceat.201900003.

[36] Niecikowska A, Zawala J, Malysa K. Influence of n-alkiltrimethylammonium bromided (C8, C12, C16) and bubble motion on kinetics of bubble attachment to mica surface. Physicochem. Probl. Miner. Process 2011;46:237–48.

[37] Sharma A, Ruckenstein E. Effects of surfactants on wave-induced drainage of foam and emulsion films. Colloid Polym. Sci. 1988;266:60–9. https://doi.org/10.1007/BF01451533/METRICS.

[38] Ivanov IB, Dimitrov DS, Somasundaran P, Jain RK. Thinning of films with deformable surfaces: diffusion-controlled surfactant transfer. Chem. Eng. Sci. 1985;40:137–50.

[39] Krzan M, Lunkenheimer K, Malysa K. Pulsation and bouncing of a bubble prior to rupture and/or foam formation. Langmuir 2003;19:6586–9. https://doi.org/10.1021/LA020919R/ASSET/IMAGES/LARGE/LA020919RF00004.JPEG.

[40] Zawala J. "Immortal" liquid film formed by colliding bubble at oscillating solid substrates. Phys. Fluids 2016:28: 057103. https://doi.org/10.1063/1.4948628.

[41] Gawel D, Zawala J. Stability of liquid films formed by a single bubble and droplet at liquid/gas and liquid/liquid interfaces in bovine serum albumin solutions. ACS Omega 2021;6:18289–99. https://doi.org/10.1021/acsomega.1c02188.

[42] Miguet J, Rouyer F, Rio E. The Life of a Surface Bubble. Molecules 2021;26(5): 13172021.

[43] Miguet J, Pasquet M, Rouyer F, Fang Y, Rio E. Stability of Big Surface Bubbles: Impact of Evaporation and Bubbles Size. Soft Matter 2020;16:1082–90. https://doi.org/10.1039/C9SM01490J.

[44] Kirkpatrick RD, Lockett MJ. The influence of approach velocity on bubble coalescence. Chem. Eng. Sci. 1974;29(12):2363–73.

[45] Manica R, Klaseboer E, Chan DYC. The impact and bounce of air bubbles at a flat fluid interface. Soft Matter 2016;12:3271–82. https://doi.org/10.1039/c5sm03151f.

[46] Manica R, Klaseboer E, Chan DYC. Force balance model for bubble rise, impact, and bounce from solid surfaces. Langmuir 2015;31:6763–72. https://doi.org/10.1021/acs.langmuir.5b01451.

[47] Kosior D, Zawala J, Malysa K. Influence of n-octanol on the bubble impact velocity, bouncing and the three phase contact formation at hydrophobic solid surfaces. Colloids Surf. A Physicochem. Eng. Asp. 2014;441: 788–795. https://doi.org/10.1016/j.colsurfa.2012.10.025.

[48] Zawala J, Dabros T. Analysis of energy balance during collision of an air bubble with a solid wall. Phys. Fluids 2013:25: 123101. https://doi.org/10.1063/1.4847015.

[49] Fujasová-Zedníková M, Vobecká L, Vejrazka J. Effect of solid material and surfactant presence on interactions of bubbles with horizontal solid surface. Can. J. Chem. Eng. 2010;88:473–81. https://doi.org/10.1002/cjce.20326.

[50] Zednikova M, Crha J, Vobecká L, Basařová P, Vejrazka J, Tihon J. Collision of bubbles with solid surface in the presence of specific surfactants. Minerals 2021; vol 11:442. https://doi.org/10.3390/MIN11050442.

[51] Suñol F, González-Cinca R. Rise, bouncing and coalescence of bubbles impacting at a free surface. Colloids Surf. A Physicochem. Eng. Asp. 2010;365:36–42. https://doi.org/10.1016/J.COLSURFA.2010.01.032.

[52] Sato A, Shirota M, Sanada T, Watanabe M. Modeling of bouncing of a single clean bubble on a free surface. Phys. Fluids 2011;23:013307. https://doi.org/10.1063/1.3546019.

[53] Manica R, Hendrix MHW, Gupta R, Klaseboer E, Ohl CD, Chan DYC. Effects of hydrodynamic film boundary conditions on bubble–wall impact. Soft Matter 2013;9:9755–8. https://doi.org/10.1039/C3SM51769A.

[54] Tsao HK, Koch DL. Observations of high Reynolds number bubbles interacting with a rigid wall. Phys. Fluids 1997;9:44–56. https://doi.org/10.1063/1.869168.

[55] Canot É, Davoust L, el Hammoumi M, Lachkar D. Numerical simulation of the buoyancy-driven bouncing of a 2-D bubble at a horizontal wall. Theor. Comput. Fluid Dyn. 2003;17:51–72. https://doi.org/10.1007/S00162-003-0096-Y/METRICS.

[56] Zawala J, Dorbolo S, Vandewalle N, Malysa K. Bubble bouncing at a clean water surface. Phys. Chem. Chem. Phys. 2013;15:17324–32. https://doi.org/10.1039/c3cp52746h.

[57] Zawala J, Dorbolo S, Terwagne D, Vandewalle N, Malysa K. Bouncing bubble on a liquid/gas interface resting or vibrating. Soft Matter 2011;7:6719–26. https://doi.org/10.1039/c1sm05365e.

[58] Zawala J, Wiertel A, Niecikowska A, Malysa K. Influence of external vibrations on bubble coalescence time at water and oil surfaces—Experiments and modelling. Colloids Surf. A Physicochem. Eng. Asp. 2017:519:137–145. https://doi.org/10.1016/j.colsurfa.2016.05.054.

[59] Zenit R, Legendre D. The coefficient of restitution for air bubbles colliding against solid walls in viscous liquids. Phys. Fluids 2009;21:083306. https://doi.org/10.1063/1.3210764.

[60] Legendre D, Daniel C, Guiraud P. Experimental study of a drop bouncing on a wall in a liquid. Phys. Fluids 2005;17:097105. https://doi.org/10.1063/1.2010527.

[61] Krasowska M, Krzan M, Malysa K. Bubble collisions with hydrophobic and hydrophilic surfaces in alpha-terpineol solutions. Physicochem. Probl. Miner. Process. 2003;37:37–50.

[62] Legendre D, Zenit R, Daniel C, Guiraud P. A note on the modelling of the bouncing of spherical drops or solid spheres on a wall in viscous fluid. Chem. Eng. Sci. 2006;61:3543–9. https://doi.org/10.1016/J.CES.2005.12.028.

[63] Joseph GG, Zenit R, Hunt ML, Rosenwinkel AM. Particle–wall collisions in a viscous fluid. J. Fluid Mech. 2001;433:329–46. https://doi.org/10.1017/S0022112001003470.

[64] Vakarelski IU, Yang F, Thoroddsen ST. Free-rising bubbles bounce more strongly from mobile than from immobile water-air interfaces. Langmuir 2020;36: 5908–18. https://doi.org/10.1021/ACS.LANGMUIR.0C00668/ASSET/IMAGES/LARGE/LA0C00668_0008.JPEG.

[65] Krasowska M, Malysa K. Time scale of the three-phase contact formation by the bubble colling with hydrophobic surface in n-pantenol and n-octanol solutions. Physicochem. Probl. Miner. Process. 2005;39:21–32.

[66] Kowalczuk PB, Zawala J, Kosior D, Drzymala J, Malysa K. Three-phase contact formation and flotation of highly hydrophobic polytetrafluoroethylene in the presence of increased dose of frothers. Ind. Eng. Chem. Res. 2016;55:839–43. https://doi.org/10.1021/acs.iecr.5b04293.

[67] Kosior D, Zawala J, Krasowska M, Malysa K. Influence of n-octanol and α-terpineol on thin film stability and bubble attachment to hydrophobic surface. Phys. Chem. Chem. Phys. 2013:15 :2586–2595. https://doi.org/10.1039/c2cp43545d.

[68] Kosior D, Zawala J, Todorov R, Exerowa D, Malysa K. Bubble bouncing and stability of liquid films formed under dynamic and static conditions from n-octanol solutions. Colloids Surf. A Physicochem. Eng. Asp. 2014:460: 391–400. https://doi.org/10.1016/j.colsurfa.2013.11.022.

[69] Wang S, Guo T, Dabiri S, Vlachos PP, Ardekani AM. Effect of surfactant on bubble collisions on a free surface. Phys. Rev. Fluids 2017;2:043601. https://doi.org/10.1103/PHYSREVFLUIDS.2.043601/FIGURES/8/MEDIUM.

[70] Sharma PK, Dixit HN. Energetics of a bouncing drop: Coefficient of restitution, bubble entrapment, and escape. Phy. Fluids 2020;32:112107.

[71] Borkowski M, Zawala J. Influence of temperature on rising bubble dynamics in water and n-pentanol solutions. Minerals 2021:11: 1067. https://doi.org/10.3390/min11101067.

[72] Zawala J, Niecikowska A. "Bubble-on-demand "generator with precise adsorption time control. Rev. Sci. Instrum. 2017:88: 095106. https://doi.org/10.1063/1.5001846/962889.

[73] Frostad JM, Tammaro D, Santollani L, Bochner de Araujo S, Fuller GG. Dynamic fluid-film interferometry as a predictor of bulk foam properties. Soft Matter 2016; 12:9266–79. https://doi.org/10.1039/C6SM01361A.

[74] Chandran Suja V, Kannan A, Kubicka B, Hadidi A, Fuller GG. Bubble coalescence at wormlike micellar solution-air interfaces. Langmuir 2020;36:11836–44. https://doi.org/10.1021/acs.langmuir.0c01861.

[75] Chandran Suja V, Rodríguez-Hakim M, Tajuelo J, Fuller GG. Single bubble and drop techniques for characterizing foams and emulsions. Adv. Colloid Interf. Sci. 2020;286:102295. https://doi.org/10.1016/j.cis.2020.102295.

[76] Fainerman VB, Möbius D, Reinhard Miller. Surfactants: chemistry, interfacial properties, applications661; 2001.

[77] Fainerman VB, Miller R, Aksenenko EV, Makievski AV. Equilibrium adsorption properties of surfactant solutions single and mixed. Studies in Surface Science 2001;13:189–285.

[78] Ward AFH, Tordai L. Time-dependence of boundary tensions of solutions i. The role of diffusion in time-effects. J. Chem. Phys. 2004;14:453. https://doi.org/10.1063/1.1724167.

[79] Ulaganathan V, Krzan M, Lotfi M, Dukhin SS, Kovalchuk VI, Javadi A, et al. Influence of β-lactoglobulin and its surfactant mixtures on velocity of the rising bubbles. Colloids and Surfaces A. 2014;460:361–8.

[80] Kracht W, Finch JA. Effect of frother on initial bubble shape and velocity. Int. J. Miner. Process. 2010;94:115–20. https://doi.org/10.1016/j.minpro.2010.01.003.

[81] Prosperetti A. Bubbles. Phys. Fluids 2004;16:1852–65. https://doi.org/10.1063/1.1695308.

[82] Zenit R, Magnaudet J. Path instability of rising spheroidal air bubbles: A shape-controlled process. Phys. Fluids 2008;20:061702. https://doi.org/10.1063/1.2940368.

[83] Veldhuis C, Biesheuvel A, van Wijngaarden L. Shape oscillations on bubbles rising in clean and in tap water. Phys. Fluids 2008;20:040705. https://doi.org/10.1063/1.2911042.

[84] Tomiyama A, Celata GP, Hosokawa S, Yoshida S. Terminal velocity of single bubbles in surface tension force dominant regime. Int. J. Multiphase Flow 2002;28:1497–519. https://doi.org/10.1016/S0301-9322(02)00032-0.

[85] Ern P, Risso F, Fabre D, Magnaudet J. Wake-induced oscillatory paths of bodies freely rising or falling in fluids44; 2011. p. 97–121. https://doi.org/10.1146/ANNUREV-FLUID-120710-101250.

[86] Tagawa Y, Takagi S, Matsumoto Y. Surfactant effect on path instability of a rising bubble. J. Fluid Mech. 2014;738:124–42. https://doi.org/10.1017/JFM.2013.571.

[87] Herrada MA, Eggers JG. Path instability of an air bubble rising in water. Proc. Natl. Acad. Sci. 2023;120:e2216830120. https://doi.org/10.1073/PNAS.2216830120.

[88] Cano-Lozano JC, Bohorquez P, Martínez-Bazán C. Wake instability of a fixed axisymmetric bubble of realistic shape. Int. J. Multiphase Flow 2013;51:11–21. https://doi.org/10.1016/J.IJMULTIPHASEFLOW.2012.11.005.

[89] Antepara O, Balcázar N, Rigola J, Oliva A. Numerical study of rising bubbles with path instability using conservative level-set and adaptive mesh refinement. Comput. Fluids 2019;187:83–97. https://doi.org/10.1016/J.COMPFLUID.2019.04.013.

[90] Tripathi MK, Sahu KC, Govindarajan R. Dynamics of an initially spherical bubble rising in quiescent liquid. Nat. Commun. 2015:6. https://doi.org/10.1038/ncomms7268.

[91] Mysels Karol J, Frankel Stanley, Shinoda Kozo. Soap Films: Studies of Their Thinning and a Bibliography - Google Books. https://books.google.pl/books/about/Soap_Films.html?id=9OZMAQAAIAAJ&redir_esc=y; 1959 (accessed January 19, 2023).

[92] Seiwert J, Kervil R, Nou S, Cantat I. Velocity Field in a Vertical Foam Film. Phys. Rev. Lett. 2017;118:048001. https://doi.org/10.1103/PHYSREVLETT.118.048001/FIGURES/5/MEDIUM.

[93] Lhuissier H, Villermaux E. Bursting bubble aerosols. J. Fluid Mech. 2012;696:5–44. https://doi.org/10.1017/JFM.2011.418.

[94] Miguet J, Pasquet M, Rouyer F, Fang Y, Rio E. Marginal regeneration-induced drainage of surface bubbles. Phys. Rev. Fluids 2021;6:L101601. https://doi.org/10.1103/PHYSREVFLUIDS.6.L101601/FIGURES/5/MEDIUM.

[95] Shi X, Fuller GG, Shaqfeh ESG. Instability and symmetry breaking of surfactant films over an air bubble. J. Fluid Mech. 2022;953:A26. https://doi.org/10.1017/JFM.2022.888.

[96] Poulain S, Villermaux E, Bourouiba L. Ageing and burst of surface bubbles. J. Fluid Mech. 2018;851:636–71. https://doi.org/10.1017/JFM.2018.471.

[97] Miguet J, Pasquet M, Rouyer F, Fang Y, Rio E. Stability of big surface bubbles: impact of evaporation and bubble size. Soft Matter 2020;16:1082–90. https://doi.org/10.1039/C9SM01490J.

[98] Modini RL, Russell LM, Deane GB, Stokes MD. Effect of soluble surfactant on bubble persistence and bubble-produced aerosol particles. J. Geophys. Res.-Atmos. 2013;118:1388–400. https://doi.org/10.1002/JGRD.50186.

[99] Poulain S, Bourouiba L. Biosurfactants change the thinning of contaminated bubbles at bacteria-laden water interfaces. Phys. Rev. Lett. 2018;121:204502. https://doi.org/10.1103/PHYSREVLETT.121.204502/FIGURES/4/MEDIUM.

[100] Aradian A, Raphaël E, de Gennes PG. "Marginal pinching" in soap films. Europhys. Lett. 2001;55:834. https://doi.org/10.1209/EPL/I2001-00356-Y.

[101] Howell PD, Stone HA. On the absence of marginal pinching in thin free films. Eur. J. Appl. Math. 2005;16:569–82. https://doi.org/10.1017/S095679250500625X.

[102] Atasi O, Haut B, Pedrono A, Scheid B, Legendre D. Influence of soluble surfactants and deformation on the dynamics of centered bubbles in cylindrical microchannels. Langmuir 2018;34:10048–62. https://doi.org/10.1021/ACS.LANGMUIR.8B01805.

[103] Atasi O, Legendre D, Haut B, Zenit R, Scheid B. Lifetime of surface bubbles in surfactant solutions. Langmuir 2020;36:7749–64. https://doi.org/10.1021/ACS.LANGMUIR.9B03597.

[104] Rage G, Atasi O, Wilhelmus MM, Hernández-Sánchez JF, Haut B, Scheid B, et al. Bubbles determine the amount of alcohol in Mezcal. Sci. Rep. 2020;10:1–16. https://doi.org/10.1038/s41598-020-67286-x.